Postlaunch Radiometric Validation of the Clouds and the Earth's Radiant Energy System (CERES) Proto-Flight Model on the Tropical Rainfall Measuring Mission (TRMM) Spacecraft through 1999

KORY J. PRIESTLEY, BRUCE R. BARKSTROM, ROBERT B. LEE III, AND RICHARD N. GREEN

Atmospheric Sciences, NASA Langley Research Center, Hampton, Virginia

SUSAN THOMAS, ROBERT S. WILSON, PETER L. SPENCE, JACK PADEN, D. K. PANDEY,
AND AIMAN AL-HAJJAH

Science Applications International Corporation, Hampton, Virginia

ABSTRACT

Each Clouds and the Earth's Radiant Energy System (CERES) instrument contains three scanning thermistor bolometer radiometric channels. These channels measure broadband radiances in the shortwave (0.3–5.0 μm), total (0.3–>100 μm), and water vapor window regions (8–12 μm). Ground-based radiometric calibrations of the CERES flight models were conducted by TRW Inc.'s Space and Electronics Group of Redondo Beach, California. On-orbit calibration and vicarious validation studies have demonstrated radiometric stability, defined as long-term repeatability when measuring a constant source, at better than 0.2% for the first 18 months of science data collection. This level exceeds by 2.5 to 5 times the prelaunch radiometric performance goals that were set at the 0.5% level for terrestrial energy flows and 1.0% for solar energy flows by the CERES Science Team. The current effort describes the radiometric performance of the CERES Proto-Flight Model on the Tropical Rainfall Measuring Mission spacecraft over the first 19 months of scientific data collection.

1. Introduction

As part of the National Aeronautics and Space Administration's (NASA) Earth Science Enterprise (ESE) program, science investigations of earth radiances are designed to define and model natural climate changes as well as man's impact upon climate. The Clouds and the Earth's Radiant Energy System (CERES) measurements constitute one of many datasets derived from several spacecraft sensors. To allow cross comparisons with different ESE datasets, the CERES absolute radiometric calibration is tied to the International Temperature Scale of 1990 (ITS'90). To maintain traceability to ITS'90, the CERES sensor responses are monitored both prior and subsequent to launch using built-in, in-flight calibration sources in consonance with supplemental vicarious validation studies. CERES measurements are the focus of science investigations designed to measure 1) top-of-the-atmosphere (TOA) earth radiation budget components, 2) radiative forcing properties of clouds, 3) surface radiation budget, and 4) divergence through-out the atmosphere (Wielicki et al. 1996). On 27 November 1997, the CERES Proto-Flight Model (PFM) instrument package was launched on the NASA Tropical Rainfall Measuring Mission (TRMM) spacecraft. A National Space Development Agency of Japan (NASDA) launch vehicle placed the TRMM spacecraft into a low-inclination 35°, 350-km altitude orbit. Nominal scientific data collection operations commenced on 1 January 1998.

On 1 September 1998 nominal mission operations were suspended due to the failure of an onboard voltage converter to properly regulate its line voltage. The suspect converter regulates a +28-V signal arriving from the spacecraft supply bus to a constant +15-V supply for the CERES data acquisition assembly (DAA) electronics. A NASA Tiger Team, formed in September 1998, identified possible causes for the regulator degradation and assessed the risk of continued sensor operations. Chapman and Bockman (1999) have demonstrated the survivability of the DAA electronics under these types of overvoltage conditions. The CERES Science Team identified the top scientific priority as obtaining overlapping measurements with the CERES Flight Models 1 and 2 that will be launched in late 1999 aboard NASA's *Terra* spacecraft. Based upon the Tiger

Corresponding author address: Dr. Kory J. Priestley, MS 420, NASA Langley Research Center, Hampton, VA 23681-0001.
E-mail: k.j.priestley@larc.nasa.gov

Team's recommendations and the Science Team's goals, the Proto-Flight Model was operational on a limited basis from September 1998 until the launch of NASA's *Terra* spacecraft. These operations have been in support of 1) special field campaigns whose goals are to measure surface and atmospheric radiation such as INDOEX in March of 1999 and Nauru99 from 15 June to 15 July 1999, 2) intercomparisons with both NASA's Earth Radiation Budget Experiment (ERBE) nonscanner instrument on the Earth Radiation Budget Satellite spacecraft and the French Scanner for Radiation Budget (ScaRaB) instrument on the Russian *Resurs* spacecraft, and 3) radiometric stability checks of the CERES PFM sensor responses. It is anticipated that full operational status will be restored to the Proto-Flight Model in January 2000.

2. CERES instrument

Each CERES instrument package consists of a scanning thermistor bolometer sensor assembly, an elevation axis drive system, an azimuth axis drive system, and associated electronics. The CERES instruments have been designed, manufactured, and tested by TRW Inc.'s Space and Electronics Group, Spacecraft and Technology Division of Redondo Beach, California. Each flight model contains three radiometric sensors that measure the earth-reflected solar radiance in the 0.3–5.0-μm spectral region, earth-reflected and earth-emitted radiances in the 0.3–>100-μm spectral region, and earth-emitted longwave radiances in the 8–12-μm spectral region. The three sensors are coaligned and mounted on a spindle that scans about the elevation axis. This assembly may also be commanded to simultaneously rotate around the azimuth axis at rates of between 4° and 6° s^{-1}. The flight models have a mass of less than 45.6 kg and consume less than 50 W of power dining nominal flight operations.

Each sensor consists of a telescope containing a forward baffle, Cassegrain optics, and a thermistor bolometer detector module assembly composed of active and reference detectors. The f/1.8 Cassegrain optics module has 18- and 8-mm diameter spherical silvered primary and secondary mirrors. In the shortwave and window sensor units, filters are located before the secondary mirror ''spider'' (the name applied to the three-legged structure that supports the secondary mirror) and in front of the active bolometer detector. The shortwave sensor filter pair consists of 1.02- and 0.51-mm-thick fused, waterless quartz elements (Si0$_2$), while the 8–12-μm window filter system consists of a 1-mm-thick zinc sulfide and a 0.5-mm-thick cadmium telluride filter element. At nadir, the 1.3° × 2.6° sensor field of view (small dimension is in the elevation scan direction) corresponds to a geographical footprint of approximately 10 km for the TRMM spacecraft orbital altitude of 350 km.

In the detector module assembly, the active and reference detectors are mounted on separate aluminum heatsinks that are in thermal contact via a 100-μm sputtered indium interface and actively maintained at a constant temperature of 38°C. This design simplifies thermal control by maintaining the assembly at temperatures greater than the surroundings allowing energy deposited on the detectors to diffuse to surrounding structure.

A black layer on the active detector absorbs the target scene energy and converts it into sensible heat causing a measurable change of the electrical resistance in the thermistor layer of the active detector. Each thermistor is a sintered semiconductor material with a high negative coefficient of electrical resistance, B. The electrical resistance R can be represented as a function of the local temperature T by (Astheimer 1983):

$$R = R_o \exp\left[B\left(\frac{1}{T} - \frac{1}{T_o}\right)\right], \qquad (1)$$

where R_o is the electrical resistance in ohms (Ω) at the reference temperature T_o (K). The active bolometer responds to thermal energy from the desired scene while the reference detector compensates for variations in the sensor thermal environment. Both detectors are in adjacent arms of a Wheatstone bridge and the output signal is passed through a low-noise preamplifier low-pass filter before entering a four-pole Bessel filter, after which it is sampled.

3. Data reduction algorithms

CERES radiance measurements are filtered measurements represented theoretically by

$$I_f^j = \int_0^\infty S_\lambda^j I_\lambda \, d\lambda \qquad j = \text{tot, wn, sw,} \qquad (2)$$

where S_λ is the spectral response of a given radiometric channel (total, window, or shortwave), I_λ is the spectral radiance incident to the instrument aperture, and I_f^j is the radiance absorbed by the detector. For a Cassegrain optical system such as CERES, S_λ may be represented as

$$S_\lambda = \rho_\lambda^2 \tau_\lambda \alpha_\lambda, \qquad (3)$$

where ρ_λ represents the spectral reflectance of each of the two silver mirrors, τ_λ is the spectral transmission of any optical filters, and α_λ is the spectral absorptance of the absorber layer of the detector. Priestley et al. (1998) presents the procedure of determining S_λ for the CERES sensors. Figure 1 displays the spectral response functions utilized in the CERES Proto-Flight Model Edition 1 ERBE-like data products.

In order to preserve continuity with ERBE long-term datasets, the initial CERES data reduction algorithms have followed the procedures developed for ERBE. The filtered radiance (W m^{-2} sr^{-1}) measured by each sensor unit can be expressed by (Lee et al. 1998)
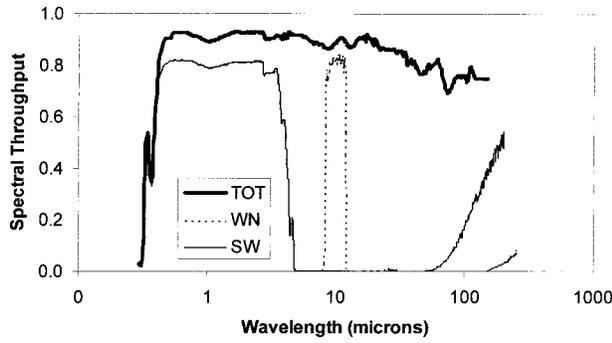
FIG. 1. CERES PFM Edition 1 spectral response functions.

$$I_f^j(t - \tau) = A_V[m(t) - \overline{m}(t_k) - o(t)]$$

$$+ \frac{t - t_k}{\Delta t}\{A_S[\overline{m}(t_{k+1}) - m(t_k)]$$

$$+ A_H[T_H(t_{k+1}) - T_H(t_k)]$$

$$+ A_D[V_D(t_{k+1}) - V_D(t_k)]$$

$$+ A_B[V_{\text{bias}}(t_{k+1}) - V_{\text{bias}}(t_k)]\}, \quad (4)$$

where

$$t_{k+1} = t_k + \Delta t,$$

and Δt is equal to 6.6 s. In (4) τ represents the time lag between the instantaneous optical pointing vector and point spread function centroid as determined prelaunch by Paden et al. (1998) and verified postlaunch by Currey et al. (1998), $o(t)$ represents the scan position dependent offset term in digital counts as determined by Thomas et al. (1998), $m(t)$ the instrument output signal in digital counts at time t, and $\overline{m}(t_k)$ the mean instrument output signal when viewing cold space at the start of a given scan, k. By subtracting the instrument output signal of cold space, $\overline{m}(t_k)$, from earth-viewing samples, the CE-RES instrument obtains a highly accurate measurement of terrestrial and solar energy flows relative to a near-zero (2.7 K) constant temperature blackbody source (Turner 1993). The radiometric gain term A_V converts changes in the thermal state of the detecting element, represented by digital counts, into an equivalent absorbed radiance. The gain term A_S properly accounts for any drift in the absolute detector signal between subsequent space looks. Theory demonstrates that the value of the A_S coefficient is equal in magnitude, but opposite in sign to that of A_V. The remaining gain terms A_H, A_D, and A_B remove potential contamination of detector output due to both thermal and electrical contamination originating from varying heatsink temperatures, T_H, digital-to-analog converter (DAC) bridge balance voltages, V_D, and detector bias voltages, V_{bias}.

The thermal and electrical design of the CERES Proton-Flight Model instrument has reduced both the variations and sensitivity to variations, of the heatsink temperature, T_H, bias voltage, V_{bias}, and DAC bridge balance voltage, V_D, to levels that are negligible during normal operations. Thus (4) reduces to the first two terms on the right-hand side for nominal operational scenarios. The current effort presents the stability of both the A_V coefficient and spectral response S_λ for the CERES PFM instrument.

Ground characterization testing revealed that the sensor's radiometric output $m(t)$ is affected by a small transient at the ~1% level. Modeling studies demonstrate that this transient is caused by diffusion of thermal energy from the active to the compensating bolometer through the heatsink. In the data processing system, a numerical filter is used to account for this transient. Since the transient consists of a single slow mode whose time constant is on the order of 300 ms, its response $v(t)$ can be computed at time t in terms of its previous level at time $(t - \delta t)$, and the sensor output voltage $m(t)$ can be characterized by the following recursive equation:

$$v(t) = p_o v(t - \delta t) - p_1 m(t). \quad (5)$$

The slow mode is subtracted from the sensor output voltage to yield the transient-corrected sensor output voltage $u(t)$ as

$$u(t) = \frac{[m(t) - v(t)]}{1 - c}. \quad (6)$$

The filter weights p_o and p_1 are given by

$$p_o = \exp\left(\frac{-\zeta\delta t}{1 + c}\right) \quad (7)$$

$$p_1 = \frac{c(1 - p_o)}{1 + c}, \quad (8)$$

where $1/\zeta$ is equal to the characteristic time of the slow mode and c is the response of the slow mode to a unit step input. Values of ζ and c for the CERES PFM instrument may be seen in Table 1. To assess the stability of the prelaunch values listed in Table 1, on 19 March 1999 the PFM instrument was placed in an operational mode in which the radiometric channels were allowed

TABLE 1. Radiometric gain and slow-mode filter coefficients for the CERES PFM instrument as determined during ground calibration.

		Shortwave channel	Total channel	Window channel
Radiometric gain term	A_v (W m^{-2} sr^{-1} count^{-1})	0.10005	0.15056	0.10978
	A_s (W m^{-2} sr^{-1} count^{-1})	−0.10005	−0.15056	−0.10978
Slow mode coefficients	ζ (s)	0.1189	0.2447	0.2395
	c (—)	0.013	0.016	0.013

to stare first at cold space and then at the internal calibration sources with an approximately 2-s dwell at each. Analysis of this data demonstrated no detectable changes from the prelaunch values.

The A_V and A_S terms are determined by regressing sensor counts, heatsink temperature measurements, bias voltage levels, and DAC voltage levels against the calculated filtered radiances, respectively. Ground-based radiometric calibration of the CERES Proto-Flight Model instrument was conducted using a state-of-the-art Radiometric Calibration Facility (RCF) designed and built by TRW (Jarecke et al. 1991). Among the many features of the RCF are unique longwave and shortwave calibration systems. The primary infrared standard is a narrow-field blackbody (NFBB) whose temperature knowledge is traceable to the ITS'90 via seven platinum resistance thermometers (PRTs). A unique shortwave reference source consisting of an internal optical bench and filter wheel, integrating sphere, and quartz–tungsten–halogen lamp source provides stable, well-characterized radiometric sources in 14 narrow bands between 0.4 and 2.0 μm. A cryogenically cooled transfer active cavity radiometer allows traceability of calibration in the 0.4–2.0-μm region to ITS'90 (Folkman et al. 1994). Radiometric gain values, as determined during the ground-based radiometric calibration, may be seen in Table 1.

On-orbit calibration monitoring strategies include the use of onboard calibration equipment and vicarious validation studies. Onboard calibration equipment consists of an internal calibration module (ICM) and a solar calibration assembly. Vicarious validation studies include a three-channel intercomparison that allows an empirical measure of the relative magnitude and stability of the spectral response functions for both the shortwave channel and shortwave portion of the total channel.

4. Postlaunch calibration monitoring strategies

On-orbit calibrations are designed to monitor and quantify traceability to the ground-measured radiometric gain terms that will be revised only if changes larger than 0.5 percent in the longwave region, or 1 percent in the shortwave region are detected and verified. Vicarious validation studies using earth radiance measurements may either verify or dismiss sensor response changes indicated by ICM and solar calibrations. Detailed analyses of the first 19 months of in-flight calibrations and validation studies are completed.

a. Calibration monitoring systems

Two different calibration systems whose heritage and performance are traceable to ERBE scanner instruments are resident in each CERES flight model. The primary ICM carries the ground calibration radiometric scale into orbit for all three channels and provides longwave stability measurements over the mission lifetime. The ICM system consists of 2.75-cm-diameter, concentric grooved, anodized aluminum blackbody sources for the total and window channel sensors, and an evacuated tungsten lamp source, known as the shortwave internal calibration source (SWICS), for the shortwave sensor. Since the ICM radiometric scale is traceable to the NFBB in the RCF via embedded PRTs, a full broadband infrared (i.e., >5 μm) recalibration is possible on-orbit.

During internal calibration sequences, the blackbodies are maintained at three distinct temperature levels between ambient and 40 K above ambient (285, 305, and 325 K). For PFM, the nominal, heaters off, blackbody temperature varies between 286 and 293 K resulting in only two controlled blackbody temperature levels. In January 1999, the lowest level was redefined in the flight software as 295 K allowing three actively controlled levels to be realized. Sensor output is regressed against the theoretical blackbody filtered radiances to monitor the broadband longwave radiometric stability of the total and window channels.

Temperature knowledge is obtained via two PRTs embedded in the blackbody structure. Before and after being placed in the blackbodies, the PRTs are calibrated in temperature-controlled oil baths to determine coefficients used in the Callendar Van Deusen PRT equation. Initial measurements were made by the PRT manufacturer, Rosemount Inc., subsequent to thermal cycling procedures that replicate the bond curing process used by TRW when attaching the PRTs to the blackbodies. After attaching the PRTs, TRW immersed the PRT/blackbody assembly in a temperature-controlled oil bath to verify the coefficients. Thus, the ICM blackbodies radiometric scales are based upon their embedded PRTs. Transfer of the RCF's NFBB PRT-based radiometric scale onto the ICM blackbodies using the CERES sensors as transfer standards has been completed.

The SWICS resides in the ICM and consists of an evacuated tungsten lamp, associated optics, and an independent silicon photodiode (SiPD) detector. The lamp (WAMCO, Inc., Part OL-715A S15 TPL-09) has operating specifications of 5.0 V, 0.115 A, with a peak output of 0.15 candela centered at $\sim$1.0 μm. The system operates at four discrete radiance levels between 0 and 400 W m^{-2} sr^{-1}. These levels correspond to filament current levels of 0, 0.0669, 0.0925, and 0.1080 A. The SiPD detector subsystem (manufactured by EG&G, Inc.) contains a narrowband multilayer SiO$_2$–TiO$_2$ dielectric filter allowing independent narrowband lamp stability measurements centered at 746.2 nm with a full-width at half-maximum bandwidth of 104.2 nm. To ensure lamp stability once installed in the instrument, burn-in periods of a minimum of 96 h were conducted on all flight units.

Two additional abbreviated life tests on a total of four lamps were conducted to quantify stability. The initial test was run on a single WAMCO lamp to make preliminary assessments. For this test the lamp was oper-

ated for 880 h (37 days) at 97% of its design current and power cycled daily. Results suggested broadband radiometric stability at 0.3% as measured with germanium and silicon detectors (Folkman and Flannery 1993). In the second test, three flight lamps were selected at random and operated for 142 total hours to measure both broad- and narrowband radiant stabilities. The narrow band was defined by the SiO_2–TiO_2 filter in the SiPD detector subassembly, while the broad band was defined by the shortwave channel bandpass filter. Results demonstrated that of the three test samples one met the specification of narrow- and broadband radiant stability of better than $\pm 0.3\%$. One sample met the criteria for the broadband specification but not the narrow band, the third sample failed to meet specification in both bands, and drifted by as much as 1.44% in the narrow band (Hedman 1993). Lee et al. (1993) reports that lamps used on the ERBE instruments demonstrated brightness shifts as much as 1 percent over mission lifetime, and the SiPDs demonstrated responsivity shifts as large as 6 percent. Clouse (1991) documented SiPD degradation due to gamma radiation exposure in the space environment.

The second onboard system, the mirror attenuator mosaic (MAM), monitors long-term on-orbit stability of both the shortwave and shortwave portion of the total channels using solar radiances reflected from the MAM diffuser plates. The diffuser plates consist of an array of spherical aluminum mirror segments separated by a Merck Black paint overcoated with a silicon dioxide reflecting surface. Thermistors located in each diffuser plate and field-of-view limiting baffle quantify the emitted thermal longwave energy that must be accounted for in the total channel solar calibration measurements. Folkman et al. (1993) provides an in-depth overview of the MAM subsystem's design.

Solar calibration procedures include measurements of the diffuser plate before the sun drifts into the field of view, when the sun is in the field of view, and after the sun has drifted out from the field of view. During this period the sensors scan between and dwell on the diffuser plate, ICM, and cold space. The ICM sources are not activated during the solar calibrations.

During the first 30 days in orbit, the CERES instrument contamination doors remained closed, and calibration sequences were conducted daily using the ICM. Since the contamination doors were closed, the measurements were referenced to the low-emittance aluminum interior walls of the doors. The surface temperatures, and thus the emitted infrared energy, of these walls varied significantly over the time period of an orbit and they failed to provide an adequately stable referencing source.

Earth radiance measurements were initiated subsequent to the opening of the contamination doors on the 30th day in orbit. Thereafter all radiance measurements, including the ICM and solar calibrations, are referenced to observations of cold space. ICM and solar calibra-

tions were performed daily during the first week of earth radiance measurements, every other day during the second week, and once a week for the third and fourth weeks. Thereafter calibrations have been performed every 14th day during normal operations. ICM measurements for time periods when the contamination doors were closed are not discussed in this effort.

b. Vicarious validation studies

Although the ICM and solar calibrations provide the primary measurements of radiometric stability, it is also necessary to perform ancillary empirical validation studies using measured earth radiances to either support or refute results determined from the onboard equipment. Green and Avis (1996) have developed vicarious calibration validation techniques that encompass interchannel comparisons. Kratz et al. (2000, manuscript submitted to *J. Geophys. Res.*) has also developed methodologies to compare theoretical atmospheric radiative transfer models (Kratz and Rose 1999) to validate instrument response. Since only a single CERES instrument has been launched to date, modified versions of the Green and Avis interchannel comparisons have been applied to the CERES PFM instrument.

THREE-CHANNEL INTERCOMPARISON

The three-channel intercomparison is based upon inherent redundancy in the three CERES channels. Assuming an appropriate narrow- to broadband conversion may be determined to convert the 8–12-μm window channel into a "synthetic" longwave channel (i.e., 5–>100 μm) shortwave radiances may then be determined by either the shortwave channel or the difference between the total and synthetic longwave channel. Similarly, the longwave radiance may also be determined by subtracting the shortwave channel from the total channel, and the total radiance may be determined by summing the shortwave and synthetic longwave channel.

The narrow- to broadband conversion is accomplished by regressing the nighttime window channel measurements against the nighttime total channel broadband radiance for the same footprints. Because there is potentially a large amount of uncertainty in estimating the broadband longwave radiance from a narrow window radiance we have limited this analysis to nadir footprints comprised entirely of deep convective clouds (DCCs) whose brightness temperatures are less than 215 K. Since DCCs exist only at high altitudes (>10 km), we have minimized uncertainties due to atmospheric scattering and water vapor absorption, and the resulting relationship is statistically robust. Daytime longwave measurements for DCCs are then obtained by both the narrow- to broadband conversion of window channel measurements and by subtracting shortwave channel measurements from total channel measurements. By re-
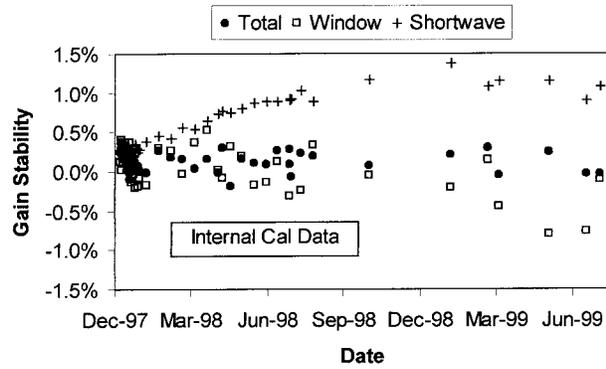
FIG. 2. On-orbit radiometric stability of the CERES PFM radiometric channels as determined with the ICM. All values are normalized to ground calibration data.
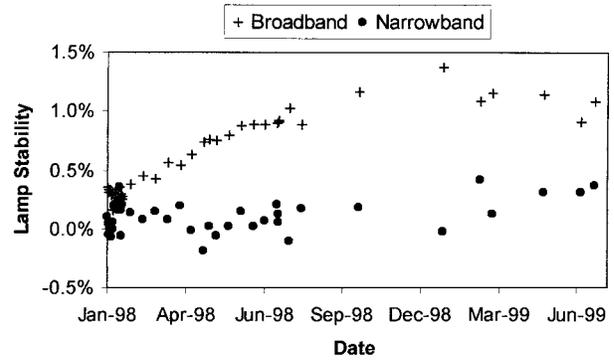

FIG. 3. SWICS tungsten lamp narrow- (0.6–0.85 μm) and broadband- (0.3–5.0 μm) stability measurements for the CERES PFM.

gressing the difference of these two daytime longwave radiance values against the daytime filtered shortwave measurements, both inconsistencies and changes in the relationship between the estimated spectral response of the shortwave channel and shortwave portion of the total channel may be seen.

Since the spectral weighting of solar energy reflected off of DCCs is a weak function of solar zenith angle, uncertainties in unfiltering the shortwave radiances are minimized. Implicit assumptions in this method are that emitted longwave radiance is independent of solar zenith angle and that the algorithms used in determining the spectral unfiltering coefficients are applied consistently to both the shortwave channel and shortwave portion of the total channel.

It can be shown (see the appendix) that the three-channel intercomparison technique empirically assesses the relationship between the true spectral response functions of the total and shortwave channels and our best estimates of these functions as determined during the radiometric ground calibrations. It does not assess the absolute accuracy of either channel. Any disagreement between truth and estimate may be quantified by

$$ \text{error} = \left(\frac{\dfrac{\hat{a}^{\text{sw}}}{\hat{a}^{\text{sw/tot}}} - \dfrac{a^{\text{sw}}}{a^{\text{sw/tot}}}}{\dfrac{\hat{a}^{\text{sw}}}{\hat{a}^{\text{sw/tot}}}} \right) = -\frac{\left(\dfrac{d\Delta}{dI_f^{\text{sw}}}\right)100}{\hat{a}^{\text{lw/tot}}\left(\dfrac{\hat{a}^{\text{sw}}}{\hat{a}^{\text{sw/tot}}}\right)}, \quad (9) $$

where Δ is the daytime longwave difference; I_f^{sw} is the daytime filtered shortwave measurement; and $\hat{a}^{\text{sw}}$, $\hat{a}^{\text{sw/tot}}$, and $\hat{a}^{\text{lw/tot}}$ are our estimates of the true spectral unfiltering coefficients a^{sw}, $a^{\text{sw/tot}}$, and $a^{\text{lw/tot}}$.

From (A9) in the appendix we have shown that the filtered shortwave radiance as measured by the total channel may be estimated from the filtered shortwave measurement as

$$ \hat{I}_f^{\text{sw/tot}} = \frac{\hat{a}^{\text{sw}}I_f^{\text{sw}}}{\hat{a}^{\text{sw/tot}}} + \frac{\hat{b}^{\text{sw}}}{\hat{a}^{\text{sw/tot}}} - \frac{\hat{b}^{\text{sw/tot}}}{\hat{a}^{\text{sw/tot}}}. \quad (10) $$

For CERES, $\hat{b}^{\text{sw}} \approx \hat{b}^{\text{sw/tot}} \ll \hat{I}_f^{\text{sw/tot}}$ so that from (10) we get

$$ \frac{\hat{a}^{\text{sw/tot}}}{\hat{a}^{\text{sw}}} \cong \frac{I_f^{\text{sw}}}{\hat{I}_f^{\text{sw/tot}}} \cong \frac{\displaystyle\int_0^\infty \hat{S}_\lambda^{\text{sw}} I_\lambda \, d\lambda}{\displaystyle\int_0^\infty \hat{S}_\lambda^{\text{sw/tot}} I_\lambda \, d\lambda}. \quad (11) $$

Solving the integral in (11) yields a value of 1.12 for DCC. A negative error from (9) would imply the right-hand side of (11) is too small and thus either $\hat{S}_\lambda^{\text{sw}}$ is low or $\hat{S}_\lambda^{\text{sw/tot}}$ is high. A positive error would imply the opposite. Since the shortwave CERES data products are derived from shortwave channel measurements only, errors in $\hat{S}_\lambda^{\text{sw/tot}}$ will not affect these products. We have no indication from this validation test whether $\hat{S}_\lambda^{\text{sw}}$ or $\hat{S}_\lambda^{\text{sw/tot}}$ is incorrect. Moreover, even if it was known which estimate was in error, there is no information of the error as a function of λ since our tests were on the integrals of S_λ over λ.

5. Results

Lifetime radiometric stability of the CERES PFM sensors as determined with the ICM may be seen in Fig. 2. Flight radiometric gain values were determined from the postenvironmental ground-based radiometric calibrations conducted by TRW in September 1995. Data from December 1997 and later correspond to on-orbit internal calibration procedures where the contamination doors are open. All data points in Fig. 2 are referenced to the final three internal calibration sequences conducted during ground calibrations. Ground to initial on-orbit traceability of the absolute calibration is 0.13, 0.14, and 0.26 percent for the total, window, and shortwave channels with 95% confidence bounds of 0.05, 0.07, and 0.01 percent. Values were determined by comparing results of the final three internal calibrations conducted during ground calibrations to the mean value determined using the ICM for the period of 27 December 1997–27 January 1998 for the total and window channels and 27
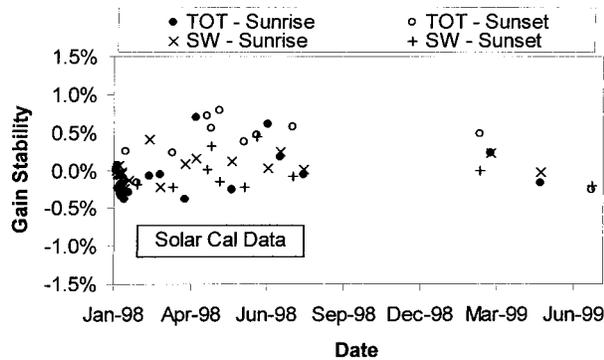
FIG. 4. On-orbit radiometric stability of the CERES PFM total and shortwave radiometric channels as determined using solar calibration techniques. Values are normalized to the initial on-orbit solar calibration event.

TABLE 2. Three-channel intercomparison results for the CERES PFM Edition 1 data products.

Month in 1998	Slope (%)	Error (%)	95% confidence interval about the error
Jan	0.72	−0.57	0.022
Feb	0.70	−0.55	0.029
Mar	0.84	−0.66	0.025
Apr	0.88	−0.70	0.029
May	0.88	−0.70	0.028
Jun	0.94	−0.74	0.027
Jul	0.85	−0.67	0.024
Aug	0.87	−0.68	0.025

December 1997–6 January 1998 for the shortwave channel.

On-orbit radiometric stability for the window and longwave portion of the total channel as determined by analyzing measurements from the ICM blackbodies may also be seen in Fig. 2. Regression analyses of the on-orbit ICM gains demonstrates the total channel sensor remained stable at the 0.03-percent level ($<$0.1 W m^{-2}) with a 0.10-percent 95% confidence bound. The window channel sensor remained stable at the 0.22-percent level ($<$0.15 W m^{-2}) with a 0.17-percent 95% confidence bound over the first 8 months of science data collection (January–August 1998). Data subsequent to August 1998 corresponds to short (less than 24 h) operations in support of field campaigns and intercalibrations with the ScaRaB instrument. The CERES detectors require thermal stability levels that are not fully realized in the 24 h subsequent to activation. The resulting bias variations of approximately 0.1–0.5 percent in the window channel measurements during the September 1998 to July 1999 time frame are visible in Fig. 2. These bias values are consistent with the known theoretical relationship between radiometric gain and detector substrate temperature for thermistor bolometer detectors (Astheimer 1983). Archived data products for these operations have the production strategy "Transient_Ops" in their naming convention and the bias is documented in CERES Data Quality Summaries, which data users must sign prior to ordering any CERES products.

Figure 2 also shows a drift in the SWICS lamp radiance level of approximately 1 percent over the same dataset from March 1998 to July 1999 as measured by the shortwave sensor. Figure 3 displays both the broad- and narrowband stability levels of the SWICS tungsten lamp as measured by the shortwave sensor and SiPD suggesting that the change was outside the SiPD's spectral bandpass. Ground characterization testing of lamp specimens demonstrated relative instability at the 1-percent level. Clouse (1991) shows the responsivity of the SiPDs is known to degrade as a result of gamma radiation damage in the space environment, and Lee et al. (1993) demonstrated that for ERBE this degradation of the SiPD responsivity was as much as 6 percent over 5 yr. If the SiPD responsivity were to decrease simultaneously with a brightening of the lamp, the resultant time series of narrowband SiPD measurements could appear stable as in Fig. 3.

On-orbit radiometric stabilities for the shortwave and shortwave portion of the total channels determined from solar calibrations utilizing the MAM assemblies have been described in detail by Wilson et al. (1998) and may be seen in Fig. 4. Regression analyses show gain stability in the shortwave and shortwave portion of the total channels of better than 0.07 percent ($<$0.1 W m^{-2}) and 0.28 percent ($<$0.7 W m^{-2}), respectively, with 95% confidence bounds of 0.17 and 0.34 percent over the time period of January 1998–July 1999. Larger variability in the total channel measurements is the result of not correctly removing the longwave components with the current algorithms. This may be seen when the solar calibration events are divided between sunrise and sunset events. During the sunrise events, the MAM baffles heat rapidly while during sunset events the MAM baffles cool rapidly. Algorithm errors manifest themselves as biases between the two types of events and thus increase the apparent overall variability in the total channel measurements.

The DCC scene-type used in the three-channel intercomparison occurs in less than 1 percent of the total earth-viewing measurements. This necessitates that the analysis be done on a monthly basis in order to obtain a rigorous statistical relationship in the narrow- to broadband conversion of the window channel measurement. The three-channel intercomparison analysis has been completed for the months of January–August 1998.

The three-channel intercomparison validation study provides insight not only of the relative relationship between the shortwave channel and shortwave portion of the total channel, but also the stability of this relationship over time. Table 2 presents the error, as calculated from Eq. (9), in this relationship on a monthly basis. There appears on average a summed total inconsistency in the estimates of the integrated spectral response functions, $\hat{S}_\lambda$, of the shortwave channel and

TABLE 3. Summary of the on-orbit radiometric gain stabilities (in %) at the 95% confidence level of the CERES PFM radiometric channels as measured by various calibration and validation techniques.

Technique	Shortwave channel	Total channel	Window channel
Internal calibration model	N/A (unstable lamp)	0.03 (0.10)	0.22 (0.17)
Solar calibration (MAM)	0.07 (0.17)	0.28 (0.34)	N/A
Three-channel intercomparison	0.14 (0.12)	0.14 (0.12)	N/A

shortwave portion of the total channel of 0.66 percent with a 0.023 95% confidence bound. This total error may be completely attributable to either channel or some combination of each. There is no indication from this analysis as to the distribution. If attributed to the short-wave channel, it would suggest that our estimate of the shortwave spectral response function, $\hat{S}_\lambda^{sw}$, is too low and that CERES shortwave data products are high by approximately 0.66 percent ($\sim$0.5 W m^{-2} TOA globally averaged flux). Conversely, if the error is attributed to the total channel, then our estimate of the total spectral response function is too high in the shortwave region by almost the same amount, and the CERES shortwave data products are fine. Regardless of which channel the error is attributed to, the derived longwave products are low by the same amount ($\sim$0.5 W m^{-2} TOA flux). These errors are being investigated and will be addressed with the release of the Edition 2 CERES ERBE-like data products in early 2000.

Regression of the monthly errors over the 8 months demonstrates a measured relative stability of 0.14 percent (0.15 W m^{-2} LW TOA flux) with a 0.17-percent confidence bound. Thus the ability of the CERES instruments to detect TOA flux changes at the 0.25-percent level has not been compromised. These results agree with the findings of the solar calibrations for both the shortwave and total channels, as well as the internal blackbody calibration of the total channel. Table 3 summarizes the on-orbit radiometric stabilities of the CERES PFM radiometric channels as measured by these various calibration and validation techniques.

6. Conclusions

On 27 November 1997, the CERES Proto-Flight Model (PFM) instrument package was launched on the NASA Tropical Rainfall Measuring Mission (TRMM) spacecraft. A National Space Development Agency of Japan. (NASDA) launch vehicle placed the TRMM spacecraft into a low-inclination 35°, 350-km altitude orbit. Analysis of the 19 months of on-orbit internal calibration and vicarious validation studies indicate that the ground-based radiometric calibrations that are tied to ITS'90 have been successfully carried into orbit to within 0.13, 0.14, and 0.26 percent for the total, window, and shortwave channels, respectively. Additionally, these analyses have indicated that on-orbit radiometric

stability has remained at levels of better than 0.14, 0.22, and 0.14 percent for the total, window, and shortwave channels. In global average TOA flux, these levels correspond to magnitudes of less than 0.3, 0.2, and 0.15 W m^{-2}.

The usefulness of ancillary vicarious validation studies to support or refute primary performance monitoring techniques has been demonstrated. Although the ICM and solar calibration measurements will remain the primary source of information regarding absolute radiometric performance, novel validation techniques such as the three-channel intercomparison remain necessary to completely characterize the performance envelope of space-based remote sensing instruments.

APPENDIX

Theoretical Basis of the Three-Channel Intercomparison

In order to validate the spectral response functions for the shortwave channel and shortwave portion of the total channel we have developed a three-channel intercomparison. The procedure is to use the window channel to define the broadband longwave radiance and compare this radiance to that derived from the total and shortwave channels. It will be shown that any differences in these two estimates may be attributed to errors in our estimates of the shortwave spectral response functions.

Since the total channel measures both solar-reflected and earth-emitted radiance, the filtered total channel radiance measurement may be thought of as containing both a shortwave (sw) and longwave (lw) component, or

$$I_f^{tot} \equiv I_f^{sw/tot} + I_f^{lw/tot}. \qquad (A1)$$

For nighttime measurements there is no shortwave component and thus (A1) reduces to

$$I_f^{tot}(n) = I_f^{lw/tot}(n). \qquad (A2)$$

The unfiltered longwave radiance at night may be determined by the total channel measurement as

$$\hat{I}^{lw}(n)|_{tot} = \hat{a}^{lw/tot}I_f^{tot}(n) + \hat{b}^{lw/tot}, \quad (A3)$$

where $\hat{I}^{lw}(n)|_{tot}$ is the estimate of the unfiltered longwave radiance at night as determined by the total channel; I_f^{tot} is the filtered total channel radiance measurement at night; and $\hat{a}^{lw/tot}$ and $\hat{b}^{lw/tot}$ are spectral unfiltering coefficients determined from a theoretical database of the representative spectral radiances, I_λ's, and the estimates of the total channel spectral response function, S_λ^{tot}. Green and Avis (1996), Arduini (1985), and Loeb et al. (2000) provide a thorough discussion of the theoretical spectral radiance databases.

Since CERES also contains a third infrared atmospheric window channel measurement from 8 to 12 μm, one may also estimate the broadband unfiltered longwave radiance at night with this channel. This is obtained by developing a narrow- to broadband conversion of the window channel by regressing the filtered window channel measurement, I_f^{wn}, against the unfiltered longwave radiance at night determined by the total channel, $\hat{I}^{lw}(n)|_{tot}$. The result of this regression is

$$\hat{I}^{lw}(n)|_{wn} = \hat{a}^{lw/wn}I_f^{wn}(n) + \hat{b}^{lw/wn}, \quad (A4)$$

where $\hat{a}^{lw/wn}$ and $\hat{b}^{lw/wn}$ are the regression coefficients.

For daytime measurements, the unfiltered longwave measurement is determined from the total and shortwave channels as follows:

$$\hat{I}^{lw}(d)|_{tot,sw} = \hat{a}^{lw/tot}I_f^{tot}(d) + \hat{b}^{lw/tot} - X, \quad (A5)$$

where the nighttime unfiltering coefficients give the longwave radiance plus a shortwave component that must be subtracted by X. It follows from (A1), (A2), (A3), and (A5) that

$$\hat{I}^{lw}(d)|_{tot,sw} = \hat{a}^{lw/tot}(I_f^{sw/tot}(d) + I_f^{lw/tot}(d)) + \hat{b}^{lw/tot} - X$$

$$= [\hat{a}^{lw/tot}I_f^{lw/tot}(d) + \hat{b}^{lw/tot}] + \hat{a}^{lw/tot}I_f^{sw/tot}(d)$$

$$- X = \hat{I}^{lw}(d) + \hat{a}^{lw/tot}I_f^{sw/tot}(d) - X$$

so that

$$X = \hat{a}^{lw/tot}I_f^{sw/tot}(d). \quad (A6)$$

If we knew with absolute certainty the value of S_λ for the shortwave and shortwave portion of the total channel we could precisely determine the magnitude of the shortwave component in the total channel measurement, $I_f^{sw/tot}$, utilizing the shortwave channel measurement and the following methodology. First, unfilter the shortwave channel radiance measurement by

$$I^{sw} = a^{sw}I_f^{sw} + b^{sw}, \quad (A7)$$

where a^{sw} and b^{sw} are the necessary spectral unfiltering coefficients determined for the DCC scene type. Second, "filter" this unfiltered shortwave channel measurement with the spectral unfiltering coefficients defined by the spectral response function for the shortwave part of the total channel. This provides the shortwave component of the total channel measurement $I_f^{sw/tot}$,

$$I_f^{sw/tot} = \frac{a^{sw}I_f^{sw}}{a^{sw/tot}} + \frac{b^{sw}}{a^{sw/tot}} - \frac{b^{sw/tot}}{a^{sw/tot}}. \quad (A8)$$

In practice, we only have best estimates, based on radiometric calibration data, for the spectral response functions for the three CERES radiometric channels. Therefore, we can only estimate the shortwave component given in (A8) with

$$\hat{I}_f^{sw/tot} = \frac{\hat{a}^{sw}I_f^{sw}}{\hat{a}^{sw/tot}} + \frac{\hat{b}^{sw}}{\hat{a}^{sw/tot}} - \frac{\hat{b}^{sw/tot}}{\hat{a}^{sw/tot}}. \quad (A9)$$

Thus,

$$I_f^{sw/tot} = \hat{I}_f^{sw/tot} + \varepsilon, \quad (A10)$$

where the error function ε accounts for any mistakes in our estimate of the spectral response function S_λ^j where j represents either the shortwave or total channels. Thus from (A5), (A6), and (A9) we have

$$\hat{I}^{lw}(d)|_{tot,sw} = \hat{a}^{lw/tot}I_f^{tot}(d) + \hat{b}^{lw/tot}$$

$$- \hat{a}^{lw/tot}\left(\frac{\hat{a}^{sw}I_f^{sw}}{\hat{a}^{sw/tot}} + \frac{\hat{b}^{sw}}{\hat{a}^{sw/tot}} - \frac{\hat{b}^{sw/tot}}{\hat{a}^{sw/tot}}\right). \quad (A11)$$

We can now determine the daytime longwave difference as

$$\Delta = \hat{I}^{lw}(d)|_{tot,sw} - \hat{I}^{lw}(d)|_{wn} \quad (A12)$$

and from (A1), (A4), (A8), and (A11)

$$\Delta = \hat{a}^{lw/tot}\left[\left(\frac{a^{sw}I_f^{sw}}{a^{sw/tot}} + \frac{b^{sw}}{a^{sw/tot}} - \frac{b^{sw/tot}}{a^{sw/tot}}\right) + I_f^{lw/tot}(d)\right]$$

$$+ \hat{b}^{lw/tot} - \hat{a}^{lw/tot}\left(\frac{\hat{a}^{sw}I_f^{sw}}{\hat{a}^{sw/tot}} + \frac{\hat{b}^{sw}}{\hat{a}^{sw/tot}} - \frac{\hat{b}^{sw/tot}}{\hat{a}^{sw/tot}}\right)$$

$$- [\hat{a}^{lw/wn}I_f^{wn}(d) + \hat{b}^{lw/wn}]. \quad (A13)$$

The sensitivity of the daytime longwave difference to the filtered shortwave measurement is defined as

$$\frac{d\Delta}{dI_f^{sw}} = -\hat{a}^{lw/tot}\left(\frac{\hat{a}^{sw}}{\hat{a}^{sw/tot}} - \frac{a^{sw}}{a^{sw/tot}}\right), \quad (A14)$$

where the second term in parentheses is the true ratio of the spectral responses of the shortwave channel and the shortwave portion of the total channels and the first term in the parentheses is our estimate of this ratio. The three-channel intercomparison provides us with the left-hand side of (A14). The percent error in our estimate of the ratio is

$$error = \left|\frac{\frac{\hat{a}^{sw}}{\hat{a}^{sw/tot}} - \frac{a^{sw}}{a^{sw/tot}}}{\frac{\hat{a}^{sw}}{\hat{a}^{sw/tot}}}\right|100 = -\frac{\left(\frac{d\Delta}{dI_f^{sw}}\right)}{\hat{a}^{lw/tot}\left(\frac{\hat{a}^{sw}}{\hat{a}^{sw/tot}}\right)}100.$$

$$(A15)$$

REFERENCES

Arduini, 1985: Solar radiance models for determination of ERBE scanner filter factor. Contractor Rep. 172595, 26 pp. [Available from NASA Langley Research Center, Hampton, VA 23681.]

Astheimer, R. W., 1983: Thermistor infrared detectors. *Proc. SPIE,* **443,** 95–109.

Chapman, J. J., and J. Bockman, 1999: Assessment of selected CERES electronic component survivability under overvoltage conditions. *Proc. SPIE,* **3750,** 494–502.

Clouse, L. G., 1991: SWICS Silicon Photodiode. TRW Interoffice Correspondence, IOC# CERES.93.750.093T, 12 pp. [Available from NASA Langley Research Center, Hampton, VA 23681.]

Currey, J. C., G. L. Smith, and B. Neely, 1998: Evaluation of the Clouds and the Earth's Radiant Energy System (CERES) scanner pointing accuracy using a coastline detection system. *Proc. SPIE,* **3439,** 367–376.

Folkman, M. A., and M. Flannery, 1993: Results of the CERES Shortwave In-Flight Calibration Source (SWICS) lamp evaluation testing. TRW Interoffice Correspondence IOC CERES.92.610.020T, 12 pp. [Available from NASA Langley Research Center, Hampton, VA 23681.]

——, P. J. Jarecke, T. R. Hedman, J. S. Yun, and R. B. Lee III, 1993: Design of a solar diffuser for on-orbit calibration of the Clouds and the Earth's Radiant Energy (CERES) instrument. *Proc. SPIE,* **1939,** 72–81.

——, and Coauthors, 1994: Calibration of a shortwave reference standard by transfer from a blackbody standard using a cryogenic active cavity radiometer. *Proc. IGARSS'94,* Pasadena CA, IGARSS, 2298–2300.

Green, R. N., and L. M. Avis, 1996: Validation of ERBS scanner radiances. *J. Atmos. Oceanic Technol.,* **13,** 851–862.

Hedman, T., 1993: CERES SWICS lamp life test-radiometric evaluation For FTM. TRW Interoffice Correspondence IOC CERES.93.620.006T, 15 pp. [Available from NASA Langley Research Center, Hampton, VA 23681.]

Jarecke, P. J., M. A. Folkman, and L. A. Darnton, 1991: Radiometric calibration plan for the Clouds and the Earth's Radiant Energy System (CERES) scanning instruments. *Proc. SPIE,* **1493,** 244–254.

Kratz, D. P., and F. G. Rose, 1999: Accounting for molecular absorption within the spectral range of the CERES window channel. *J. Quant. Spectrosc. Radiat. Transfer,* **61,** 83–95.

Lee, R. B., III, L. M. Avis, M. A. Gibson, S. Thomas, and R. Wilson, 1993: In-flight evaluations of tungsten calibration lamps using shortwave thermistor bolometers and active-cavity radiometers. *Metrologia,* **30,** 389–395.

——, and Coauthors, 1998: Prelaunch Calibrations of the Clouds and the Earth's Radiant Energy System (CERES) Tropical Rainfall Measuring Mission and Earth Observing System Morning (EOS-AM1) spacecraft thermistor bolometer sensors. *IEEE Trans. Geosci. Remote Sens.,* **36,** 1173–1185.

Loeb, N. G., K. J. Priestley, D. P. Kratz, E. B. Geier, R. N. Green, B. A. Wielicki, P. O. Hinton, and S. K. Nolan, 2000: Determination of unfiltered radiances from the Clouds and the Earth's Radiant Energy System (CERES) instrument. *J. Appl. Meteor.,* in press.

Paden, J., G. L. Smith, R. B. Lee III, D. K. Pandey, K. J. Priestley, H. C. Bitting, S. Thomas, and R. S. Wilson, 1998: Comparisons between point response function measurements and theory for the Clouds and the Earth's Radiant Energy System (CERES) TRMM and the EOS-AM spacecraft thermistor bolometer sensors. *Proc. SPIE,* **3439,** 344–354.

Priestley, K. J., B. R. Barkstrom, H. Bitting, R. B. Lee III, D. K. Pandey, S. Thomas, and K. L. Thornhill, 1998: End-to-end spectral characterization of the Clouds and the Earth's Radiant Energy System (CERES) thermistor bolometer radiometers. *Proc. SPIE,* **3498,** 12–22.

Thomas, S., and Coauthors, 1998: Flight and ground calibrations: TRMM and EOS-AM1 Clouds and the Earth's Radiant Energy System (CERES) instrument zero radiance offsets determination. *Proc. SPIE,* **3429,** 315–324.

Turner, M. S., 1993: Why is the temperature of the universe 2.726? *Science,* **262,** 861–867.

Wielicki, B. A., B. R. Barkstrom, E. F. Harrison, R. B. Lee III, G. L. Smith, and J. E. Cooper, 1996: Clouds and the Earth's Radiant Energy System (CERES): An Earth Observing System experiment. *Bull. Amer. Meteor. Soc.,* **77,** 853–868.

Wilson, R. S., and Coauthors, 1998: On-orbit solar calibrations using the TRMM Clouds and the Earth's Radiant Energy System (CERES) in-flight calibration system. *Proc. SPIE,* **3429,** 325–334.